AIAA JOURNAL
Vol. 39, No. 2, February 2001

Vibration of Pretwisted Adaptive Rotating Blades Modeled as Anisotropic Thin-Walled Beams

Ohseop Song*
Chungnam National University, Taejon 305-764, Republic of Korea
Liviu Librescu†
Virginia Polytechnic Institute and State University, Blacksburg, Virginia 24061
and
Sang-Yong Oh‡
Chungnam National University, Taejon 305-764, Republic of Korea

Problems related to mathematical modeling and dynamic behavior of pretwisted adaptive rotating blades are considered. The blade is modeled as a thin-wall, single-cell beam encompassing nonclassical effects such as anisotropy, transverse shear, and warping restraint. The adaptive capabilities provided by a system of piezoactuators bonded or embedded into the structure are also implemented in the system. Based on the converse piezoelectric effect and of out-of-phase activation, boundary control moments are piezoelectrically induced at the beam tip. Two feedback control laws relating the induced bending moments with the appropriately selected kinematical response quantities are used, and the beneficial effects of the implementation of the active feedback control, considered in conjunction with that of the structural tailoring on the eigenvibration characteristics, are highlighted.

Introduction

ROTOR blades are vital and critical components of jet engines, turbomachinery, tilt rotor aircraft, and helicopters. A thorough understanding of dynamic characteristics of rotating blades is essential toward determining their fatigue life and avoiding catastrophic failures. The accurate determination of dynamic characteristics is also essential toward a rational prediction of their forced response, resonant behavior, and flutter instability characteristics.

The design of advanced rotor blades was significantly influenced by the incorporation of composite material technology. As compared to their metallic counterparts, composite design of rotor blades offers considerable advantages with respect to strength and weight criteria, in addition to providing adequate means of efficiently controlling static and dynamic response via implementation of structural tailoring.

An important step toward the rational design of modern rotor blades and propellers consists of the development of analytical models that are capable of accurately predicting their dynamic behavior. Moreover, to enhance their dynamic behavior and avoid vibration-induced fatigue failure, new technologies have to be implemented. One way to accomplish such goals consists of incorporation of adaptive materials technology into the host structure. In contrast to traditional passive structures, in those featuring adaptive capabilities, the natural frequencies, damping, and mode shapes can be tuned to avoid structural resonance and to enhance dynamic response characteristics. In addition, due to the nature of intelligent structures, which feature a highly distributed network of sensors and actuators, more encompassing control schemes would be feasible to be implemented. For helicopter and tilt rotor aircraft, the incorporation of adaptive materials technology for vibration control could result in significant increases in comfort, range, fatigue life, etc. In this sense, piezoelectric materials are excellent candidates for the role of sensors and actuators.

Presented as Paper 99-1550 at the AIAA/ASME/ASCE/AHS/ASC 40th Structures, Structural Dynamics, and Materials Conference and AIAA/ASME/AHS Adaptive Structures Forum on Non-Deterministic Approaches, St. Louis, MO, 12–15 April 1999; received 10 May 1999; revision received 4 May 2000; accepted for publication 30 July 2000.

*Professor, Mechanical Engineering Department.
†Professor, Department of Engineering Science and Mechanics.
‡Graduate Student, Mechanical Engineering Department.

Within this study, the free vibration of pretwisted rotating beams featuring transverse bending–lateral bending–transverse shear couplings and incorporating the adaptive capability referred to as strain actuation is investigated. The adaptive capability is achieved through the converse piezoelectric effect consisting of the generation of localized strains in response to an applied voltage. The induced strain field produces, in turn, an adaptive change in the dynamic response characteristics of the structure.

Implementation of a control law relating the applied electric field to one of the mechanical quantities characterizing the blade response according to a prescribed functional relationship results in an eigenvalue problem. Its solution supplies the closed-loop eigenvalues that are functions of the applied voltage, that is, of the feedback control gain. Under consideration is a blade rotating with constant angular velocity and modeled as a single-cell, pretwisted, thin-/thick-walled beam. Although of an evident practical importance, to the best of the authors' knowledge no studies related to the topic of this investigation can be found in the specialized literature. Even for the nonadaptive case, the literature devoted to the free-vibration problem of rotating composite blades modeled as thin-walled beams reveals an extreme paucity of results. The available survey papers[1–5] summarizing the achievements in problems related to this topic demonstrate this fact. The goal of this paper is just to fill the existing gap in the literature and to supply pertinent information in this area. The results obtained herein constitute a generalization and continuation of those previously obtained in Refs. 6–12.

Structural Model: Basic Assumptions

The case of a straight pretwisted flexible beam of length L rotating with the constant angular velocity Ω normal to the plane of rotation is considered. The origin of the rotating axis system (x, y, z) is located at the blade root at an offset R_0 from the rotation axis fixed in space. R_0 is also the radius of the hub (considered to be rigid) in which the blade is mounted and which rotates about its polar axis through the origin O (see Fig. 1). Besides the coordinates x, y, and z, we also define the local coordinates x^p, y^p, and z^p, where x^p and y^p are the principal axes of an arbitrary beam cross section.[7]

The two coordinate systems are related by the following transformation formulas:

$$x(s, z) = x^p \cos\beta - y^p \sin\beta \tag{1a}$$

$$y(s, z) = x^p \sin\beta + y^p \cos\beta \tag{1b}$$

$$z(s) = z^p \tag{1c}$$

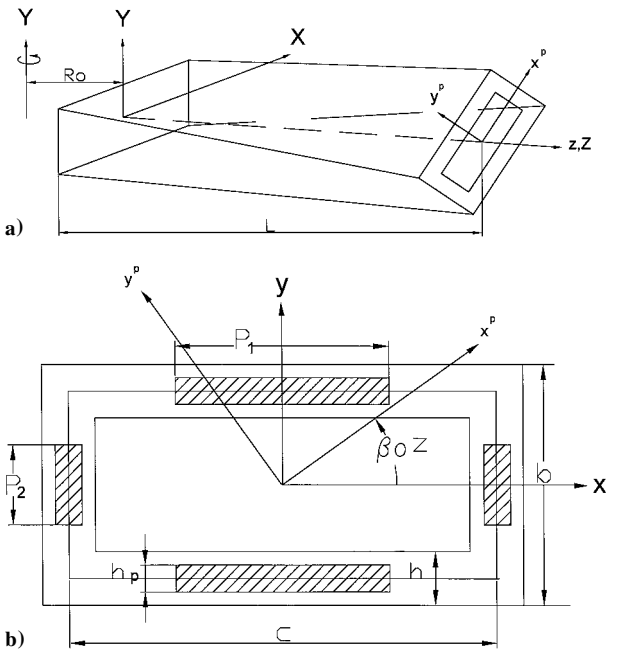

Fig. 1 Geometry of the pretwisted beam and its cross section with the embedded piezoactuators.

where $\beta = \beta_0 \bar{z}$ is the pretwist of the current section $z = \bar{z}$, whereas β_0 is the pretwist per unit beam length.

The inertial reference system (X, Y, Z) is attached to the center of the hub O. By $\boldsymbol{i}$, $\boldsymbol{j}$, and $\boldsymbol{k}$ and $\boldsymbol{I}$, $\boldsymbol{J}$, and $\boldsymbol{K}$, we define the unit vectors associated with the frame coordinates x, y, and z and X, Y, and Z, respectively. In addition, a local (surface) coordinate system (s, z, n) associated with the beam is considered. Its geometric configuration and the typical cross section along with the associated system of coordinates are presented in Figs. 1a and 1b. The precone and presetting angles of the blade are assumed to be zero. It is further assumed that the rotation takes place in the plane (X, Z) with the constant angular velocity $\boldsymbol{\Omega}(\equiv\ \Omega\boldsymbol{J} = \Omega\boldsymbol{j})$, with the spin axis along the Y axis. The structural model corresponds to a thin-/thick-walled beam. In this context, the case of a single-cell, thin-walled beam (TWB) of uniform closed section is considered, where the spanwise, z coordinate axis coincides with a straight unspecified reference axis.

Toward its modeling, the following assumptions are adopted:

1) The original cross-section shape of the beam is preserved.

2) Both primary and secondary (thickness) warping effects are included.

3) Transverse shear, rotatory inertia and centrifugal acceleration effects are included.

4) A special layup inducing flapping–lagging coupling, on one hand, and twist–extension coupling, on the other hand, is implemented.

Kinematics

In light of assumptions 1–4 and to reduce the three-dimensional elasticity problem to an equivalent one-dimensional one, the components of the displacement vector are represented as[10–12]

$$u(x, y, z; t) = u_0(z; t) - y\phi(z; t) \tag{2a}$$

$$v(x, y, z; t) = v_0(z; t) + x\phi(z; t) \tag{2b}$$

$$w(x, y, z; t) = w_0(z; t) + \theta_x(z; t)\left[y(s) - n\frac{\mathrm{d}x}{\mathrm{d}s}\right] + \theta_y(z; t) \times \left[x(s) + n\frac{\mathrm{d}y}{\mathrm{d}s}\right] - \phi'(z; t)[F_\omega(s) + na(s)] \tag{2c}$$

In these equations, $u_0(z; t)$, $v_0(z; t)$, and $w_0(z; t)$ are the rigid-body translations along the x, y, and z axes, whereas $\phi(z; t)$ and $\theta_x(z; t)$ and $\theta_y(z, t)$ are the twist about the z axis and the rotations about the x and y axes, respectively. The expressions of θ_x and θ_y as well as of the geometric quantity $a(s)$ are

$$\theta_x(z; t) = \gamma_{yz}(z; t) - v_0'(z; t) \tag{3a}$$

$$\theta_y(z; t) = \gamma_{xz}(z; t) - u_0'(z; t) \tag{3b}$$

$$a(s) = -y(s)\frac{\mathrm{d}y}{\mathrm{d}s} - x(s)\frac{\mathrm{d}x}{\mathrm{d}s} \tag{3c}$$

In Eqs. (2), $F_\omega(s)$ and $na(s)$ are primary and secondary warping functions, respectively. For their definition, see Refs. 6–9, for example.

It is readily seen that, by virtue of Eqs. (2) and (3), the statement of the cross-sectional nondeformability (implying $\epsilon_{xx} = 0$, $\epsilon_{yy} = 0$, and $\gamma_{xy} = 0$ and, consequently, $\epsilon_{nn} = \epsilon_{ss} = \gamma_{sn} = 0$) as well as the continuity requirement of w along the midline contour, that is,

$$\oint \left(\frac{\partial w}{\partial s}\right) \mathrm{d}s = 0$$

are fulfilled. It is also seen that in the absence of transverse shear effects

$$\theta_x(z; t) = -v_0'(z; t) \tag{4a}$$

$$\theta_y(z; t) = -u_0'(z; t) \tag{4b}$$

In these equations, as well as in the forthcoming ones, the primes denote differentiation with respect to the longitudinal z coordinate. The position vector of a point $M(x, y, z)$ belonging to the deformed structure is

$$\boldsymbol{R}(x, y, z; t) = (x + u)\boldsymbol{i} + (y + v)\boldsymbol{j} + (z + w)\boldsymbol{k} + \boldsymbol{R}_0 \tag{5}$$

where x, y, and z are the Cartesian coordinates of a point of the continuum in its undeformed state, whereas u, v, and w are displacement components defined through Eqs. (2). Recalling that the spin rate was assumed to be constant, with the help of equations expressing the time derivatives of unit vectors $(\boldsymbol{i}, \boldsymbol{j}, \boldsymbol{k})$, one obtains the velocity and acceleration vectors of an arbitrary point M of the beam:

$$\dot{\boldsymbol{R}} = V_x\boldsymbol{i} + V_y\boldsymbol{j} + v_z\boldsymbol{k} \tag{6a}$$

$$\ddot{\boldsymbol{R}} = a_x\boldsymbol{i} + a_y\boldsymbol{j} + a_z\boldsymbol{k} \tag{6b}$$

respectively, where their components are

$$V_x = \dot{u} + (R_0 + z + w)\Omega \tag{7a}$$

$$V_y = \dot{v} \tag{7b}$$

$$V_z = \dot{w} - (x + u)\Omega \tag{7c}$$

$$a_x = \ddot{u} + \underline{2\dot{w}\Omega} - \underline{\underline{(x + u)\Omega^2}} \tag{8a}$$

$$a_y = \ddot{v} \tag{8b}$$

$$a_z = \ddot{w} - \underline{2\dot{u}\Omega} - \underline{\underline{(R_0 + z + w)\Omega^2}} \tag{8c}$$

In these equations and the following ones, the superposed dots denote time derivatives and the terms underscored by one or two solid lines are associated with Coriolis and centrifugal inertia terms, respectively.

Equations of Motion and Boundary Conditions

Toward the goal of deriving the equations of motion of rotating beams and the associated boundary conditions, Hamilton's variational principle is used. This variational principle may be stated as[13]

$$\delta J = \int_{t_0}^{t_1} \left(\int_\tau \sigma_{ij}\delta\epsilon_{ij}\,\mathrm{d}\tau - \delta K - \int_{\Omega_\sigma} \underline{s}_i\delta v_i\,\mathrm{d}\Omega - \int_\tau \rho H_i\delta v_i\,\mathrm{d}\tau \right)\mathrm{d}t = 0 \tag{9}$$

where

$$U = \frac{1}{2}\int_{\tau} \sigma_{ij}\epsilon_{ij}\,\mathrm{d}\tau \tag{10a}$$

$$K = \frac{1}{2}\int_{\tau} \rho(\dot{\boldsymbol{R}}\cdot\dot{\boldsymbol{R}})\,\mathrm{d}\tau \tag{10b}$$

are the strain energy functional and the kinetic energy, respectively.

In these equations, t_0 and t_1 are two arbitrary instants of time, $\mathrm{d}\tau(\equiv \mathrm{d}n\,\mathrm{d}s\,\mathrm{d}z)$ is the differential volume element, and $\underline{s}_i(\equiv \underline{\sigma}_{ij}n_j)$ are the prescribed components of the stress vector on a surface element of the undeformed body characterized by the outward normal components n_i. Also, H_i are the components of the body forces, Ω_σ is the external area of the body over which the stresses are prescribed, ρ is the mass density, an undertilde sign identifies a prescribed quantity, and δ is the variation operator. In Eqs. (9) and (10) the Einstein summation convention applies to repeated indices, where Latin indices range from 1 to 3. In the same equations, $(v_1, v_2, v_3)\equiv(u, v, w)$, and $(x_1, x_2, x_3)\equiv(x, y, z)$.

In light of Eqs. (2), (5), (6), and (8), on imposing Hamilton's condition $\delta v_i = 0$ at t_0 and t_1, performing the integration over the s and n directions, one obtains for

$$\int_{t_0}^{t_1}\delta K\,\mathrm{d}t \equiv -\int_{t_0}^{t_1}\mathrm{d}t\int_{\tau}[\rho\ddot{\boldsymbol{R}}_i\cdot\delta\boldsymbol{R}_i]\,\mathrm{d}\tau$$

the expression

$$\begin{aligned}\int_{t_0}^{t_1}\delta K\,\mathrm{d}t \equiv -\int_{t_0}^{t_1}\Bigg\{&\int_0^L -\Big\{b_1\Big(\ddot{u}_0 + \underline{2\dot{w}_0\Omega} - \underline{\underline{u_0\Omega^2}}\Big)\delta u_0\\ &+ b_1\ddot{v}_0\delta v_0 + b_1\Big[\ddot{w}_0 - \underline{2\dot{u}_0\Omega} - \underline{\underline{(R_0+z+w_0)\Omega^2}}\Big]\delta w_0\\ &+ I_{yy}\Big(\ddot{\underset{\sim}{\theta}}_y - \underline{\underset{\sim}{\Omega^2\theta_y}}\Big)\delta\theta_y + \Big[I_{xx}\Big(\ddot{\underset{\sim}{\theta}}_x - \underline{\underset{\sim}{\Omega^2\theta_x}}\Big) + \underline{2I^0_{xx}\Omega\dot{\phi}}\Big]\delta\theta_x\\ &+ \Big[I_p\ddot{\phi} - \underline{2I^0_{xx}\Omega\dot{\theta}_x} - \underline{\underline{I^0_{xx}\Omega^2\phi}} - I_{\omega\omega}\Big(\ddot{\underline{\phi}}'' - \underline{\underline{\Omega^2\phi}}''\Big)\Big]\delta\phi\Big\}\,\mathrm{d}z\,\mathrm{d}t\\ &-\Big[I_{\omega\omega}\Big(\ddot{\underline{\phi}}' - \underline{\underline{\Omega^2\phi}}'\Big)\Big]\delta\phi\Big]_0^L\,\mathrm{d}t\Bigg\}\end{aligned} \tag{11}$$

Herein, for the sake of identification, in addition to the previously defined conventions, the terms associated with 1) the inertial warping, 2) the centrifugal warping, 3) rotatory inertia, and 4) centrifugal-rotatory effect are underscored by 1) one interrupted line superposed on a solid line, 2) two superposed dashed lines, 3) a dotted line, and 4) a solid line superposed on an undulated line, respectively. The expressions of structural and mass cross-sectional blade characteristics intervening in Eq. (11) have been supplied in Refs. 8 and 9 and will not be repeated here.

From Eq. (11) it becomes apparent that Coriolis acceleration constitutes a source of additional couplings between extension–lagging and flapping–twist. In the forthcoming development these terms will be discarded.

For the variation of the strain energy functional, one obtains

$$\begin{aligned}\int_{t_0}^{t_1}\int_{\tau}\sigma_{ij}\delta\epsilon_{ij}\,\mathrm{d}\tau\,\mathrm{d}t = \int_{t_0}^{t_1}\int_0^L &-\{T_z'\delta w_0 + (M_y' - Q_x)\delta\theta_y\\ &+ (M_x' - Q_y)\delta\theta_x + [\underline{B}_\omega'' + M_z' + (T_r\phi')']\delta\phi\\ &+ [Q_x' + (T_z u_0')']\delta u_0 + [Q_y' + (T_z v_0')']\delta v_0\}\,\mathrm{d}z\,\mathrm{d}t\\ &+\int_{t_0}^{t_1}\Big[T_z\delta w_0 + M_y\delta\theta_y + M_x\delta\theta_x - \underline{B}_\omega\underline{\delta}\underline{\phi}'\\ &+ (\underline{B}_\omega' + M_z + T_r\phi')\delta\phi + (Q_x + T_z u_0')\delta u_0\\ &+ (Q_y + T_z v_0')\delta v_0\Big]_0^L\,\mathrm{d}t\end{aligned} \tag{12}$$

In the preceding equations, the terms underscored by dashed lines are associated with the warping restraint effect. The equations of motion and the associated boundary conditions can be obtained from Eqs. (9–12). These equations expressed in terms of one-dimensional stress resultants T_z, Q_x, and Q_y, stress couples M_x, M_y, and M_z, and bimoment B_ω have been presented in Refs. 8 and 9 and will not be repeated here.

Governing System

The governing system of rotating elastic blades will be expressed in terms of displacement quantitites. This can be accomplished by replacing in the equations of motion and static boundary conditions the one-dimensional stress-resultants and stress-couples represented in terms of displacement quantities.

For the general case of anisotropy of constituent materials and ply-stacking sequence, the obtained governing system and the associated boundary conditions would exhibit a complete coupling between the various modes, that is, warping (primary and secondary), bending (flapping and lagging), twist, extension, and transverse shearing. The assessment of the influence of these couplings and their proper exploitation (e.g., see Refs. 10–12) should constitute an important task toward a rational design of blade structures of helicopter and tilt rotor aircraft and of the proper use of the exotic material characteristics, that is, anisotropy and ply-stacking sequence, generating these couplings.

Moreover, because of the inclusion of the pretwist, additional couplings are induced, which in such a general context would add more complexities to the problem (e.g., see Ref. 14). For these reasons, in the present analysis a special ply-angle distribution inducing the elastic coupling between flapwise bending and chordwise bending will be considered. This ply-angle distribution referred to as circumferentially uniform stiffness (CUS) configuration[15,16] is achieved by skewing angle plies with respect to the beam axis according to the law $\theta(y) = \theta(-y)$ in the top and bottom flanges and to the law $\theta(x) = \theta(-x)$ in the lateral webs. Angle θ denotes the dominant ply orientation measured from the positive s axis toward the positive z axis. On implementing this ply-angle scheme, the corresponding equations of motion and boundary conditions are obtained from the variational principle [Eq. (9)]. Employment in these equations of constitutive equations, of strain-displacement relationships, and of Eqs. (1) yields the governing equations expressed in terms of displacement quantities as

$$\begin{aligned}\delta u_0 :\ &[a_{43}(z)\theta_x' + a_{44}(z)(u_0' + \theta_y) + a_{45}(z)(v_0' + \theta_x)]' - b_1\ddot{u}_0\\ &+ \underline{b_1 u_0\Omega^2} + \underline{\underline{b_1\Omega^2[R(z)u_0']'}} = 0\end{aligned} \tag{13a}$$

$$\begin{aligned}\delta v_0 :\ &[a_{52}(z)\theta_y' + a_{55}(z)(v_0' + \theta_x) + a_{45}(z)(u_0' + \theta_y)]'\\ &- b_1\ddot{v}_0 + \underline{\underline{b_1\Omega^2[R(z)v_0']'}} = 0\end{aligned} \tag{13b}$$

$$\begin{aligned}\delta\theta_y :\ &[a_{22}(z)\theta_y' + a_{25}(z)(v_0' + \theta_x) + a_{23}(z)\theta_x']' - a_{44}(z)(u_0' + \theta_y)\\ &- a_{43}(z)\theta_x' - a_{45}(z)(v_0' + \theta_x) - [b_5(z) + b_{15}(z)]\Big(\ddot{\underset{\sim}{\theta}}_y - \underline{\underset{\sim}{\Omega^2\theta_y}}\Big)\\ &- [b_6(z) - b_{13}(z)]\ddot{\underset{\sim}{\theta}}_x = 0\end{aligned} \tag{13c}$$

$$\begin{aligned}\delta\theta_x :\ &[a_{33}(z)\theta_x' + a_{23}(z)\theta_y' + a_{34}(z)(u_0' + \theta_y)]' - a_{55}(z)(v_0' + \theta_x)\\ &- a_{52}(z)\theta_y' - a_{54}(z)(u_0' + \theta_y) - [b_4(z) + b_{14}(z)]\Big(\ddot{\underset{\sim}{\theta}}_x - \underline{\underset{\sim}{\Omega^2\theta_x}}\Big)\\ &- [b_6(z) - b_{13}(z)]\Big(\ddot{\underset{\sim}{\theta}}_y - \underline{\underset{\sim}{\Omega^2\theta_y}}\Big) = 0\end{aligned} \tag{13d}$$

From the same variational theorem, assuming the blade to be clamped at $z = 0$ and free at $z = L$, the boundary conditions result as follows:

At $z = 0$,

$$u_0 = 0 \tag{14a}$$

$$v_0 = 0 \tag{14b}$$

$$\theta_x = 0 \tag{14c}$$

$$\theta_y = 0 \tag{14d}$$

and at $z = L$

$$\delta u_0 : a_{43}(z)\theta_x' + a_{44}(z)(u_0' + \theta_y) + a_{45}(z)(v_0' + \theta_x) = 0 \quad (15a)$$

$$\delta v_0 : a_{52}(z)\theta_y' + a_{55}(z)(v_0' + \theta_x) + a_{45}(z)(u_0' + \theta_y) = 0 \quad (15b)$$

$$\delta\theta_y : a_{22}(z)\theta_y' + a_{25}(z)(v_0' + \theta_x) + a_{23}(z)\theta_x' = \hat{M}_y \quad (15c)$$

$$\delta\theta_x : a_{33}(z)\theta_x' + a_{34}(z)(u_0' + \theta_y) + a_{23}(z)\theta_y' = \hat{M}_x \quad (15d)$$

In these equations

$$R(z) \equiv \left[R_0(L - z) + \tfrac{1}{2}(L^2 - z^2)\right] \quad (16)$$

whereas the coefficients $a_{ij}(z) = a_{ji}(z)$ and $b_i(z)$ are stiffness and reduced mass terms, respectively.

Having in view all of these elements, one obtains expressions of stiffness quantities in terms of their cross-sectional principal axes x^p and y^p counterparts, which are given in the Appendix, together with those of mass terms. Equations (13) and (15) reveal that, in the context of the considered ply-angle configuration, the flapping and lagging motions are coupled with transverse shear. For this case, the stiffness quantities a_{34} and a_{25} are a reflection of this ply-angle configuration. In addition, the stiffness quantities a_{45} and a_{23} and the mass terms b_6 and b_{13}, which are different from zero only in the case of a pretwisted beam, induce a supplementary coupling between the flapping and lagging motions. However, from the expressions of a_{45}, a_{23}, b_6, and b_{13} (see the Appendix), it can readily be seen that for an axisymmetric box-beam of a square cross section, these are zero-valued quantities for any value of β. Note that in addition to the already mentioned coupling terms generated by pretwist, the remaining ones involve, as a result of pretwist, a more complex feature. Their expressions, shown in the Appendix, substantiate this statement in full.

As a result, in such a case, the flapping–lagging coupling arises independently from the pretwist effect. Notice that in addition to the elastic coupling between the flapping and lagging induced by the described ply-angle distribution and the pretwist, Eqs. (13) through (15) also feature the coupling between the flapwise shear and chordwise bending and between chordwise shear and flapwise bending. Moreover, the preceding system of governing equations also include the centrifugal and rotatory inertia effects.

Because of the inclusion of transverse shear effects, the system of Eqs. (13)–(15) belongs to the shearable beam model, whereas its classical counterpart, obtained when transverse shear effects are discarded, is referred to as the unshearable model. Notice that, via the use of the CUS ply-angle configuration, from the entire system of equilbrium equations, an additional governing equations system is obtained featuring the extension–twist coupling, decoupled from the one characterized by bending–bending–transverse shear cross-coupling. For nonpretwisted beams, the corresponding governing equations have been supplied in the Refs. 8 and 9.

Because this paper involves a study of beams featuring only transversal–lateral–bending cross coupling, the complementary system of equations involving extension–twist cross coupling will not be considered.

Nonshearable Counterpart of the Shearable Rotating Beam Model

Expressions $a_{44}(u_0' + \theta_y) + a_{45}(u_0' + \theta_x)$ and $a_{55}(v_0' + \theta_x) + a_{54}(u_0' + \theta_y)$ from Eqs. (13c) and (13d), respectively, and their corresponding replacement in Eqs. (13a), (13b), and (15a), followed by consideration of $\theta_x \to -v_0'$ and $\theta_y = -u_0'$ yield the Bernoulli–Euler counterpart of Eqs. (13–15). As a result, the governing equations are

$$\delta u_0 : [a_{22}(z)u_0'' + a_{23}(z)v_0'']'' - \left\{[b_5(z) + b_{15}(z)]\left(\ddot{\underset{\sim}{u}}_0' - \underset{\sim}{\Omega^2 u_0'}\right) + [b_6(z) - b_{13}(z)]\ddot{\underset{\sim}{v}}_0'\right\}' + b_1\ddot{u}_0 \underline{\underline{- b_1\Omega^2 u_0}} \underline{\underline{- b_1\Omega^2[R(z)u_0']'}} = 0 \quad (17a)$$

$$\delta v_0 : [a_{33}(z)v_0'' + a_{23}(z)u_0'']'' - \left\{[b_4(z) + b_{14}(z)]\left(\ddot{\underset{\sim}{v}}_0' - \underset{\sim}{\Omega^2 v_0'}\right) + [b_6(z) - b_{13}(z)]\left(\ddot{\underset{\sim}{u}}_0' - \underset{\sim}{\Omega^2 u_0'}\right)\right\} + b_1\ddot{v}_0 - \underline{\underline{b_1\Omega^2[R(z)v_0']'}} = 0 \quad (17b)$$

The associated boundary conditions are, at $z = 0$,

$$u_0 = v_0 = u_0' = v_0' = 0 \quad (18)$$

and at $z = L$

$$\delta u_0 : [a_{22}(L)u_0'' + a_{23}(L)v_0'']' - [b_5(L) + b_{15}(L)]\left(\ddot{\underset{\sim}{u}}_0' - \underset{\sim}{\Omega^2 u_0'}\right) - [b_6(L) - b_{13}(L)]\ddot{\underset{\sim}{v}}_0' = 0 \quad (19a)$$

$$\delta v_0 : [a_{33}(L)v_0'' + a_{23}(L)u_0'']' - [b_4(L) + b_{14}(L)]\left(\ddot{\underset{\sim}{v}}_0' - \underset{\sim}{\Omega^2 v_0'}\right) - [b_6(L) - b_{13}(L)]\left(\ddot{\underset{\sim}{u}}_0' - \underset{\sim}{\Omega^2 u_0'}\right) = 0 \quad (19b)$$

$$\delta u_0' : a_{22}(L)u_0'' + a_{23}(L)v_0'' = \hat{M}_y \quad (19c)$$

$$\delta v_0' : a_{33}(L)v_0'' + a_{23}(L)u_0'' = \hat{M}_x \quad (19d)$$

In this case, the flapping–lagging coupling stiffness induced by the pretwist effect is $a_{23}(z)$, and $[b_6(z) - b_{13}(z)]$ is the dynamic flapping–lagging coupling term induced by pretwist.

This procedure of reducing the governing equations of the shearable beam model to their unshearable counterpart is exact, and a similar one is used in shell/plates theory as well. An alternative approach that is implemented directly in the strain energy density function of TWB was devised in Ref. 17.

Consistent with the number of four boundary conditions at each edge, the governing equations for both shearable and unshearable pretwisted rotating beams are of order eight. A noticeable difference between the shearable and unshearable beam models is that, in the former instance, the eigenfrequencies do not intervene, in the boundary conditions at the beam tip, whereas in the latter one, they do.

Note that these terms are associated with the rotatory and centrifugal-rotatory effects, which usually are neglected. In our approach, however, these terms have been retained. Note that the nonrotating version of Eqs. (17–19) coincides with that obtained for a solid pretwisted beam in Ref. 18.

In Eqs. (15c) and (15d) and their nonshearable counterparts, Eqs. (19c) and (19d), $\hat{M}_y$ and $\hat{M}_x$ are the piezoelectrically induced bending moments about the axes y and x, respectively, which appear as nonhomogeneous terms in the boundary conditions at $z = L$. Notice that $\hat{M}_x$ and $\hat{M}_y$ are different from zero, if external voltages of opposite signs are applied in the top and bottom and in the lateral piezoactuator layers, respectively (out-of-phase activation; e.g., see Refs. 19–22).

Note that in the light of the actuator configuration, the piezoelectrically induced stress resultant and stress couples are independent on the z coordinate. As a result, in the governing equations their contribution is immaterial whereas in the boundary conditions these intervene as nonhomogeneous terms only. This feature renders the control to be accomplished via the piezoelectrically induced boundary bending moments. Notice that the boundary control constitutes a powerful way to control the static and dynamic response of structures (see Refs. 23 and 24).

Piezoactuators and Control Law

It is assumed that the master structure is composed of r layers while the actuator is composed of p piezoelectric layers. We stipulate that the actuators are distributed over the entire span of the blade, whereas along the circumferential and transverse directions, that is, along the s and n directions, they are distributed according to the law

$$P_{(k)}(n) = H\left(n - n_{(k^-)}\right) - H\left(n - n_{(k^+)}\right)$$

$$P_{(k)}(s) = H\left(s - s_{(k^-)}\right) - H\left(s - s_{(k^+)}\right) \tag{20}$$

where H is the Heaviside distribution, P is a spatial function that defines the distribution of actuators in the n and the s directions, and the subscript k identifies the affiliation of the respective quantity to the kth layer.

When it is assumed that the electric field vector $\mathcal{E}_i$ is represented in terms of its component $\mathcal{E}_3$ in the n-direction, coinciding with the direction of polarization (referred to as thickness polarization), the boundary moment controls are expressed as

$$\hat{M}_x = \oint \sum_{k=1}^{p} \mathcal{E}_3^{(k)}\left(n_{(k+)} - n_{(k-)}\right) e_{31}^{(k)} P_{(k)}(s) \times \left[y\left(1 - \frac{\hat{A}_{12}}{\hat{A}_{11}}\right) + \frac{\mathrm{d}x}{\mathrm{d}s}\frac{\hat{B}_{12}}{\hat{A}_{11}} \right] \mathrm{d}s - \frac{1}{2}\oint \left[\frac{\mathrm{d}x}{\mathrm{d}s} \sum_{k=1}^{p} \mathcal{E}_3^{(k)}\left(n_{(k+)}^2 - n_{(k-)}^2\right) e_{31}^{(k)} P_{(k)}(s) \right] \mathrm{d}s \tag{21a}$$

$$\hat{M}_y = \oint \sum_{k=1}^{p} \mathcal{E}_3^{(k)}\left(n_{(k+)} - n_{(k-)}\right) e_{31}^{(k)} P_{(k)}(s) \times \left[x\left(1 - \frac{\hat{A}_{12}}{\hat{A}_{11}}\right) + \frac{\mathrm{d}y}{\mathrm{d}s}\frac{\hat{B}_{12}}{\hat{A}_{11}} \right] \mathrm{d}s + \frac{1}{2}\oint \left[\frac{\mathrm{d}y}{\mathrm{d}s} \sum_{k=1}^{p} \mathcal{E}_3^{(k)}\left(n_{(+)}^2 - n_{(k-)}^2\right) e_{31}^{(k)} P_{(k)}(s) \right] \mathrm{d}s \tag{21b}$$

where e_{31} is the piezoelectric constant, $\hat{A}_{ij}$ and $\hat{B}_{ij}$ are the standard local-stiffness quantities associated with the piezoactuators, and $\oint(\cdot)\,\mathrm{d}s$ is the integral around the circumference of the midline cross section of the beam.

For $\mathcal{E}_3$ constant throughout the piezoactuator thickness, which implies $\mathcal{E}_3^{(k)} \equiv \mathcal{E}_3$, Eqs. (21) can be expressed in condensed form as

$$\hat{M}_x = \mathcal{E}_3 \mathcal{M}_x \tag{22a}$$

$$\hat{M}_y = \mathcal{E}_3 \mathcal{M}_y \tag{22b}$$

where the meaning of $\mathcal{M}_x$ and $\mathcal{M}_y$ becomes evident by comparing Eqs. (22) with (21).

Equations (21) reveal that the piezoelectrically induced bending moments are proportional to the applied electric current $\mathcal{E}_3$. Now, when it is assumed that the piezoelectric elements can be employed concurrently for sensing and actuation, for sensing operation the electric displacement results as

$$D_3 = e_{31} S_{zz} \tag{23}$$

and the sensor output voltage is expressed in the form[25]

$$V_s(t) = q_s(t)/C_p \tag{24}$$

where the electric charge $q_s(t)$ is

$$q_s(t) = \int_{A_s} D_3\,\mathrm{d}A_s = \int_{A_s} e_{31} S_{zz}\,\mathrm{d}A_s \tag{25}$$

C_p and A_s are the sensor's capacitance and piezoelectric patch area, respectively. When it is assumed that the sensor patches are located symmetrically on the opposite walls, that is, on $x = 0$, $y = \pm b/2$ and $y = 0$, $x = \pm c/2$, and a symmetric distribution is featured with respect to the x and y axes along the s direction and also in view of the expression of S_{zz} (Refs. 6 and 7) and Eqs. (24) and (25), $V_s^x(t)$ and $V_s^y(t)$ may be expressed as

$$V_s^x(t) = C_x^s \theta_x(L, t) \tag{26a}$$

$$V_s^y(t) = C_y^s \theta_y(L, t) \tag{26b}$$

The expressions of C_y^s and C_x^s are not shown here.

Two feedback control law strategies will be adopted, namely, 1) the proportional control law and 2) the velocity control law.

Within the first control law, one postulates that the actuating electric field is proportional to the sensor output voltage, which imples

$$\mathcal{E}_3^x(t) = K_p V_s^x(t)\big/h_a \tag{27a}$$

$$\mathcal{E}_3^y(t) = K_p V_s^y(t)\big/h_a \tag{27b}$$

whereas within the velocity feedback control law,

$$\mathcal{E}_3^x(t) = K_v \frac{\mathrm{d}V_s^x(t)/\mathrm{d}t}{h_a} \tag{28a}$$

$$\mathcal{E}_3^y(t) = K_v \frac{\mathrm{d}V_s^y(t)/\mathrm{d}t}{h_a} \tag{28b}$$

where h_a is the thickness of the piezoactuator.

Consequently, in the first case, replacement of Eqs. (27) considered in conjunction with Eqs. (26) into Eqs. (22) results in the piezoelectrically induced bending moments expressed as

$$\hat{M}_y(L, t) = \left(K_p C_{M_y^a}\big/h_a\right)\left[C_y^s \theta_y(L, t)\right] = K_p C_{11} \theta_y(L, t) \tag{29a}$$

$$\hat{M}_x(L, t) = \left(K_p C_{M_x^a}\big/h_a\right)\left[C_x^s \theta_x(L, t)\right] = K_p C_{22} \theta_x(L, t) \tag{29b}$$

In the second case of the feedback control law, replacement of Eq. (28) considered in conjunction with Eqs. (26) in Eqs. (22) yields

$$\hat{M}_y(L, t) = \left(K_v C_{M_y^a}\big/h_a\right)\left[C_y^s \dot{\theta}_y(L, t)\right] = K_v C_{11} \dot{\theta}_y(L, t) \tag{30a}$$

$$\hat{M}_x(L, t) = \left(K_v C_{M_x^a}\big/h_a\right)\left[C_x^s \dot{\theta}_x(L, t)\right] = K_v C_{22} \dot{\theta}_x(L, t) \tag{30b}$$

It is seen that the piezoelectrically induced bending moments, Eqs. (29) and (30), are obtained through the combination of both sensing and actuation functions.

Here

$$C_{M_y^a} = \sum_{k=1}^{p} e_{31}^{(k)} \left[\left(1 - \frac{\hat{A}_{11}}{\hat{A}_{11}}\right)\left(n_{(k^+)} - n_{(k^-)}\right) c + \left(n_{(k^+)}^2 - n_{(k^-)}^2\right) - 2\frac{\hat{B}_{12}}{\hat{A}_{11}}\left(n_{(k^+)} - n_{(k^-)}\right) \right] p_2 \tag{31a}$$

$$C_{M_x^a} = \sum_{k=1}^{p} e_{31}^{(k)} \left[\left(1 - \frac{\hat{A}_{11}}{\hat{A}_{12}}\right)\left(n_{(k^+)} - n_{(k^-)}\right) b + \left(n_{(k^+)}^2 - n_{(k^-)}^2\right) - 2\frac{\hat{B}_{12}}{\hat{A}_{11}}\left(n_{(k^+)} - n_{(k^-)}\right) \right] p_1 \tag{31b}$$

where p_1 and p_2 denote the lengths of the piezoactuators along the x and y directions (see Fig. 1b).

As concerns the proportional and velocity feedback gains K_p and K_v, respectively, these will be used in dimensionless form as

$$\bar{K}_p = K_p L/\hat{a}_{33} h_p \tag{32a}$$

$$\bar{K}_v = K_v L/\hat{a}_{33} h_p \tag{32b}$$

where $\hat{a}_{33}$ is the transverse bending stiffness corresponding to $\theta = 0$ and $\beta = 0$.

The coupled governing equations (13) considered in conjunction with the boundary conditions Eqs. (14) and (15), and the control law, Eqs. (29) or (30), constitutes the closed-loop eigenvalue problem related to the shearable theory of rotating thin-walled beams.

Discretized Governing Equations of Adaptive Rotating Beams

For practical purposes, it is necessary to discretize the eigenvalue-value problem. This amounts to representing u_0, v_0, θ_x, and θ_y by means of series of space-dependent trial functions multiplied by time-dependent generalized coordinates. The discretization can be

more conveniently performed via the Extended Galerkin Method (e.g., see Refs. 7, 11, 13, and 21). To this end, we express the displacements as

$$u_0(z,t) = \boldsymbol{U}_0^T(z)\boldsymbol{q}_u(t), \qquad v_0(z,t) = \boldsymbol{V}_0^T(z)\boldsymbol{q}_v(t)$$
$$\theta_x(z,t) = \boldsymbol{X}_0^T(z)\boldsymbol{q}_x(t), \qquad \theta_y(z,t) = \boldsymbol{Y}_0^T(z)\boldsymbol{q}_y(t) \tag{33}$$

where

$$\boldsymbol{U}_0(z) = [u_1 \quad u_2 \ldots u_N]^T, \qquad \boldsymbol{V}_0(z) = [v_1 \quad v_2 \ldots v_N]^T$$
$$\boldsymbol{X}_0(z) = [x_1 \quad x_2 \ldots x_N]^T, \qquad \boldsymbol{Y}_0(z) = [y_1 \quad y_2 \ldots y_N]^T \tag{34}$$

are the vectors of the space-dependent trial functions, selected to fulfill at least the geometrical boundary conditions, whereas for free-vibration problem $\boldsymbol{q}_u(t)$, $\boldsymbol{q}_v(t)$, $\boldsymbol{q}_x(t)$, and $\boldsymbol{q}_y(t)$ are represented generically as

$$\boldsymbol{F}(t) = \bar{\boldsymbol{F}}e^{\lambda t} \tag{35}$$

where $\bar{\boldsymbol{F}}$ and λ are constants, both generally complex.

In the case $\bar{K}_v \neq 0$, the solution of the algebraic eigenvalue problem yields the closed-loop eigenvalues

$$(\lambda_r, \bar{\lambda}_r) = \sigma_r \pm i\omega_{dr} \tag{36}$$

which depend on the feedback control gain $\bar{K}_v$, where σ_r is a measure of the damping in the rth mode whereas ω_{dr} is the rth frequency of the damped oscillations. The damping factor in the rth mode results as

$$\zeta_r = -\sigma_r \Big/ \left(\sigma_r^2 + \omega_{dr}^2\right)^{\frac{1}{2}} \tag{37}$$

When $\bar{K}_v = 0$ and $\bar{K}_p \neq 0$, then $(\lambda_r, \bar{\lambda}_r) = \pm i\omega_r$, and as a result, undamped free vibrations are experienced.

Numerical Simulations and Discussion

Although the obtained equations are valid for a beam of arbitrary closed cross section, for the sake of illustration the case of a rotating beam modeled as a composite box beam (see Fig. 1) characterized by a cross-sectional ratio $\mathcal{R}(\equiv c/b) = 5$ was considered. In addition, unless otherwise specified, the dimensions considered are $L = 80$ in. (2.023 m), $c = 10$ in. (0.254 m), $b = 2$ in. (50.8×10^{-3} m), $h = 0.4$ in. (10.16×10^{-3} m), and $h_p = 0.015$ in. (0.381×10^{-3} m).

Depending on whether the flapping, lagging, or flapping–lagging coupled motions are intended to be controlled, the piezoactuator layers (selected to be of PZT-4) should be located on the top and bottom flanges, on the opposite lateral webs of the master structure, or on both the flanges and webs, respectively.

Whereas the geometric characteristics of the structure are shown in Fig. 1, the properties of the PZT-4 piezoceramic may be found in Ref. 26 (pp. 202–204), and those of the host structure correspond to a graphite/epoxy material, its mechanical characteristics in the on-axis configuration are given by $E_L = 30 \times 10^6$ psi (20.68×10^{10} N/m^2), $E_T = 0.75 \times 10^6$ psi (5.17×10^9 N/m^2), $G_{LT} = 0.37 \times 10^6$ psi (2.55×10^9 N/m^2), $G_{TT} = 0.45 \times 10^6$ psi (3.10×10^9 N/m^2), $\mu_{TT} = \mu_{LT} = 0.25$, and $\rho = 14.3 \times 10^{-5}$ lb $\cdot$ s^2/in.^{4} (1528.15 kg/m^3), where subscripts L and T are directions parallel and transverse to the fiber, respectively.

Note that, in spite of the extensive work and results devoted to eigenvibration response of pretwisted rotating[27–29] and nonrotating blades modeled as solid isotropic beams and incorporating bending–bending cross coupling, (e.g., see Refs. 30–34), to the best of the authors' knowledge, there are no available results associated with both adaptive and nonadaptive anisotropic pretwisted rotating TWB.

For this reason, before presenting results revealing the effects of anisotropy coupled with that of the pretwist and of adaptive materials technology on dynamics of thin-walled rotating blades, results to be compared with the ones obtained within the solid beam model of rectangular cross sections are displayed.

Figure 2 shows the first three coupled eigenfrequencies of the nonrotating beam as a function of the pretwist angle at the beam tip. The trend of variation of ω_i vs β, as shown in Fig. 2, is similar to that

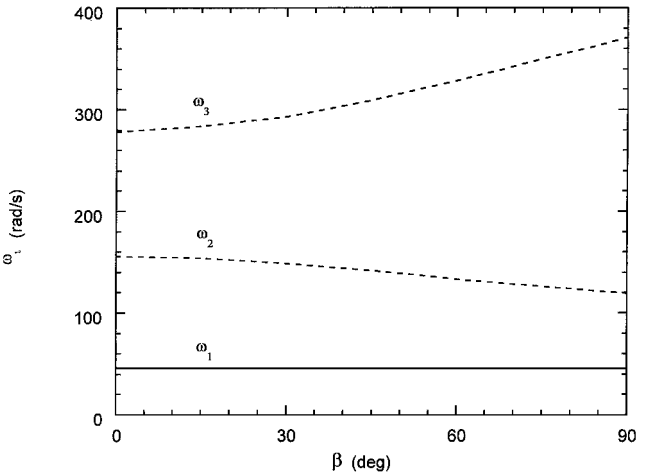

Fig. 2 Variation of first three coupled flapping and lagging natural frequencies vs pretwist angle, $\theta = 0$ deg and $\Omega = 0$ deg.

featured by a solid beam of similar $\mathcal{R}$, as reported in Refs. 29–31. Figures 3a–3c, show for selected values of the blade rotational speed, the variations of first three eigenfrequencies as a function of the pretwist angle. The trend as emerging from these plots coincides with that reported in Ref. 27 for the case of a rotating blade modeled as a solid isotropic beam.

The effect of the hub radius R_0 on the first three decoupled eigenfrequencies in flapping and lagging is shown in Figs. 4a and 4b, respectively. Whereas the emerging trend shown in Fig. 4a coincides with that reported in Ref. 35, where only the flapping motion of rotating blades was considered, the trend in Fig. 4b, revealing that the lagging eigenfrequencies are little influenced by the hub radius, appears to have not been reported yet in the literature.

The effect of transverse shear resulting in a decay of higher mode eigenfrequencies as predicted by the unshearable nonrotating beam model is shown in Fig. 5. The same trend related with the influence of transverse shear was reported for rotating solid beams in Ref. 31.

In Table 1, the effects of the chord-to-thickness ratio c/h on the first three natural frequencies ω_i (radian per second), within the shearable and unshearable box-beam models, and for the ply-angle configurations $\theta = 0$ and 90 deg are emphasized. Here ω_1(F1) and ω_3(F2) are the first consecutive frequencies in flapping, whereas ω_2(L1) is the first frequency in lagging.

The results reveal that the decrease of the chord-to-thickness ratio c/h from to 50 to 10 (implying, when c is hold fixed, a five times increase of the wall thickness) plays a very modest role toward the increase of eigenfrequencies. This trend is due to the inherent large bending stiffnesses featured by the box beam. As a result, the increase of the wall thickness yields only a slight increase of the global bending stiffness quantities.

In contrast, the tailoring technique plays a very significant role toward the increase of eigenfrequencies. In the present case, for $\theta = 90$ deg, maximum flexural stiffnesses in flapping, a_{33}, and lagging, a_{22}, are obtained that result in a notable increase of natural frequencies. This is in contrast to the ply angle $\theta = 0$ deg for which these stiffness quantities reach a minimum value.[36]

Figures 6 and 7 highlight the effects of rotational velocity Ω considered in conjunction with the implementation of the velocity feedback control strategy on the decoupled natural fundamental frequencies in flapping and lagging that occur at ply angle $\theta = 0$ deg. The results reveal that, at moderate rotational speeds, the first flapwise mode exhibits the lowest frequency. However, due to the centrifugal stiffening effect (which is much more significant in the flapping modes), beyond a certain angular speed the lagging frequency becomes the lower of the two. Figure 6 shows that, for the unactivated beam in the vicinity of $\Omega \cong 150$ rad/s, a frequency crossing of lagging and flapping modes occurs.

The results also show that for the activated beams this frequency crossing is shifted toward larger rotational velocities. Figure 7 shows, for the second frequency, the flapping–lagging frequency crossing occurs at larger values of Ω as compared to that occurring

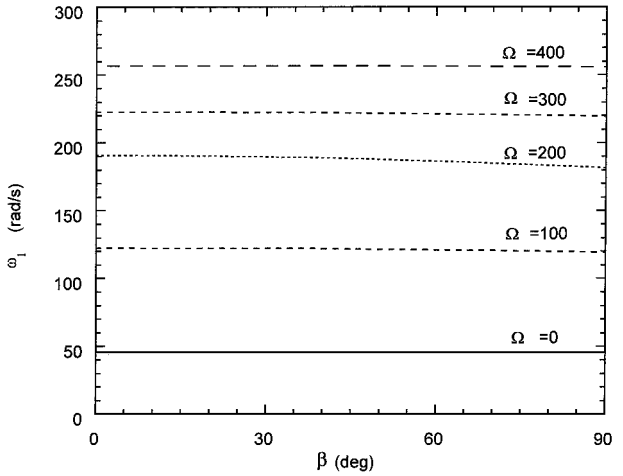

Fig. 3a Variation of first coupled flapping–lagging natural frequencies vs pretwist angle for selected rotational speeds, $\theta = 0$ deg.

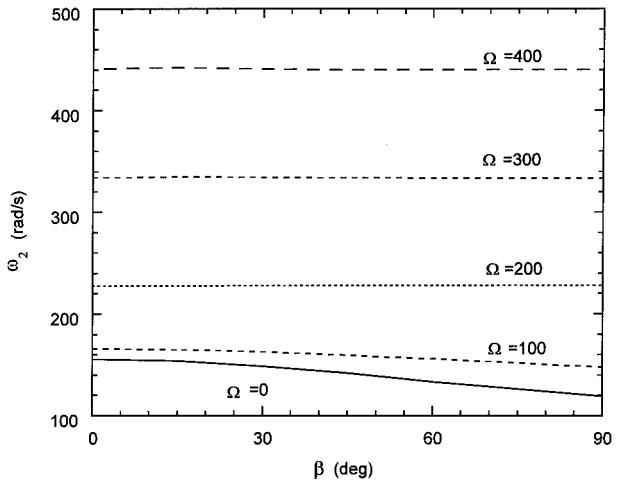

Fig. 3b Counterpart of Fig. 1a for the second coupled mode frequency.

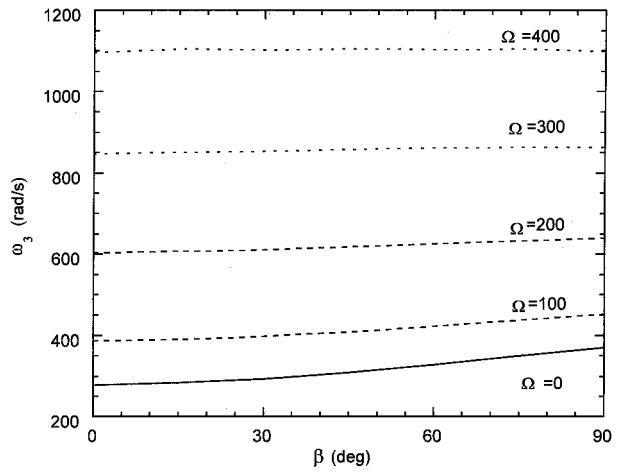

Fig. 3c Counterpart of Fig. 1a for the third coupled mode frequency.

for the fundamental frequencies. At the same time, the supplied results show that, for the ply angle $\theta = 0$ deg, the piezoelectric actuation has a more powerful effect on the lagging frequencies than on the flapping ones, whereas for $\theta = 90$ deg (see Figs. 8 and 9), the opposite trend, as compared with that emerging from Figs. 6 and 7, is observed.

In addition, for ply angle $\theta = 90$ deg, due to the larger bending stiffnesses in both flapping and lagging as induced by this ply angle,

Table 1 Effect of chord-to-thickness ratio on the natural frequencies ω_i for $\Omega = 100$ (rad/s) and $\beta = 0$ deg

Model	Frequency, rad/s	c/h = 10	20	30	40	50
		$\theta = 0$ deg				
Shearable	ω_1(F1)	120.393	119.957	119.874	119.848	119.844
	ω_2(L1)	146.901	146.845	146.834	146.83	146.828
	ω_3(F2)	367.583	362.998	362.125	361.834	361.683
Nonshearable	ω_1(F1)	120.516	120.074	119.992	119.963	119.949
	ω_2(L1)	148.166	148.107	148.096	148.093	148.091
	ω_3(F2)	369.025	364.36	363.489	363.183	363.042
		$\theta = 90$ deg				
Shearable	ω_1(F1)	265.037	259.471	258.423	258.055	257.885
	ω_2(L1)	667.59	667.396	667.359	667.347	667.341
	ω_3(F2)	1312.12	1287.78	1283.13	1281.5	1280.74
Nonshearable	ω_1(F1)	272.406	266.265	265.112	264.708	264.52
	ω_2(L1)	838.604	838.216	838.144	838.119	838.107
	ω_3(F2)	1564.91	1523.2	1515.34	1512.58	1511.3

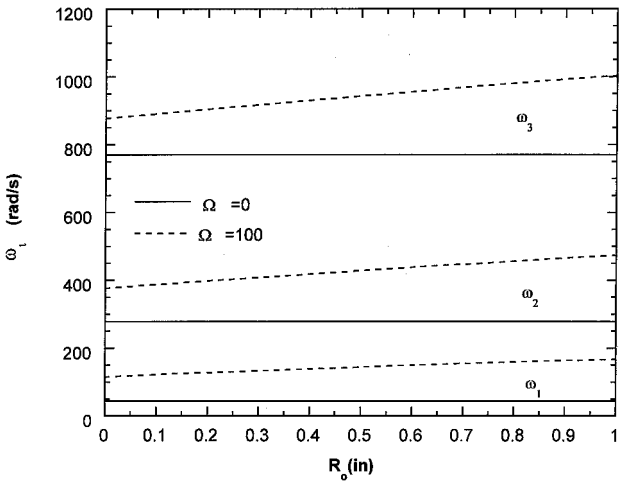

Fig. 4a Effect of hub radius on the first three decoupled flapping natural frequencies for both rotating and nonrotating blade.

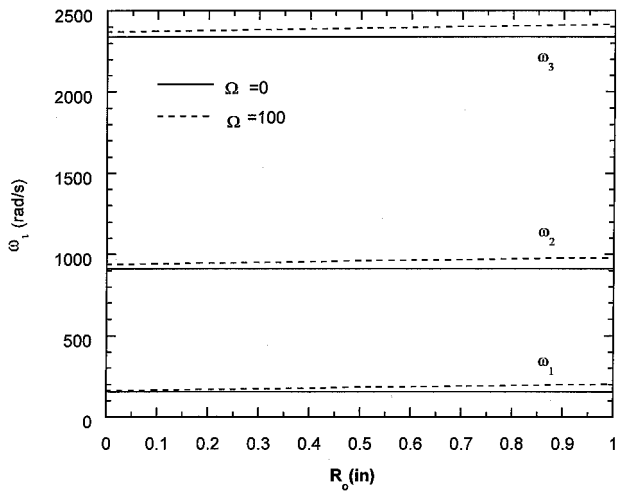

Fig. 4b Counterpart of Fig. 4a for the case of lagging natural frequencies.

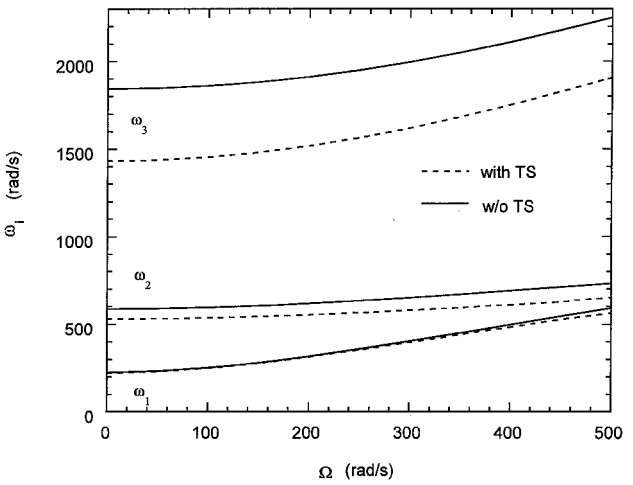

Fig. 5 Effect of transverse shear on the first three coupled natural frequencies; $\theta = 90$ deg and $\beta = 90$ deg.

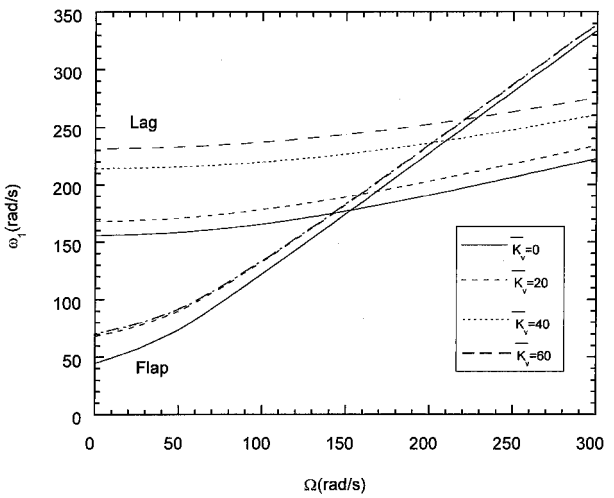

Fig. 6 Variation of first decoupled flapping and lagging natural frequencies vs rotational speed for selected $\bar{K}_v$; $\theta = 0$ deg and $\beta = 0$ deg.

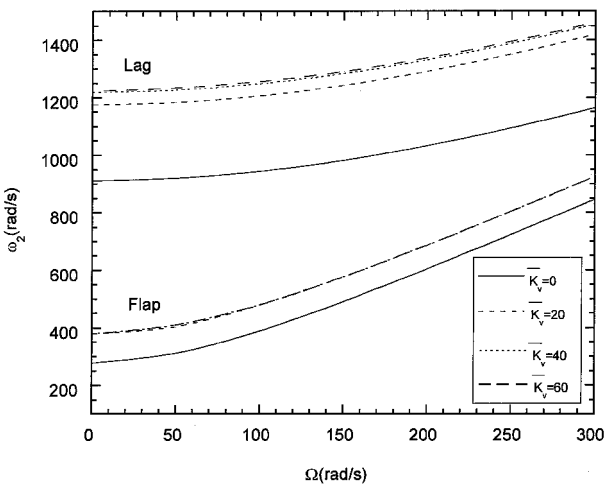

Fig. 7 Variation of second decoupled flapping and lagging natural frequencies vs rotational speed for selected $\bar{K}_v$; $\theta = 90$ deg and $\beta = 0$ deg.

the frequencies are much larger within the entire range of rotational speeds as compared to their counterparts for $\theta = 0$ deg. Also, the frequency crossing takes place at much larger rotational speeds for both the unactivated and activated rotor blade. In the case of higher modes (Fig. 9), the frequencies remain separated in the usual range of rotational speeds, in the sense that no frequency crossings occur in that range. Recall that, via velocity feedback control, induced damping is generated.

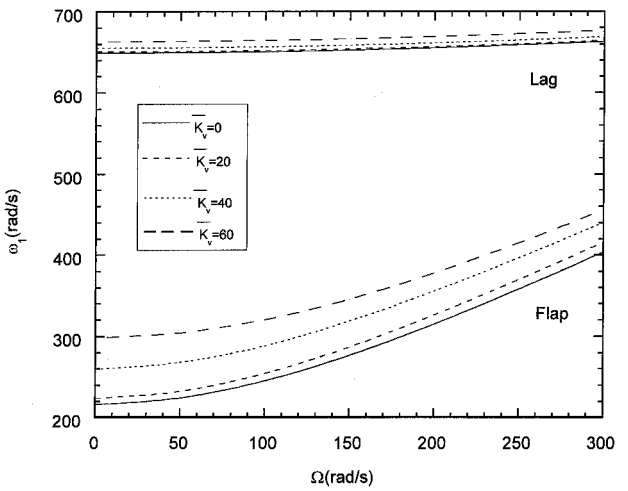

Fig. 8 Variation of first decoupled flapping and lagging natural frequencies vs rotational speed for selected $\bar{K}_v$; $\theta = 90$ deg and $\beta = 0$ deg.

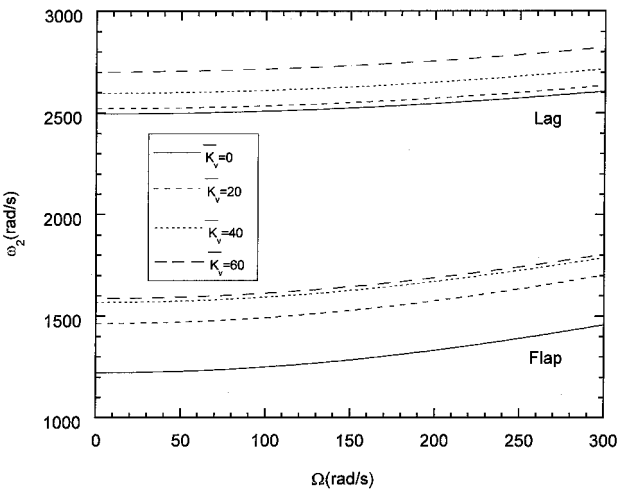

Fig. 9 Variation of second decoupled flapping and lagging natural frequencies vs rotational speed for selected $\bar{K}_v$; $\theta = 90$ deg and $\beta = 0$ deg.

Figures 10 and 11 show the induced damping factors ζ_r associated with the decoupled motions in flapping and lagging, respectively. It is seen that the increase of ζ_r with $\bar{K}_v$ takes place until a certain value of the feedback gain, specific to each mode number. Beyond that specific value of $\bar{K}_v$, referred to as the optimum feedback gain, a sharp drop of ζ_r is experienced.

This trend is consistent with that reported, in different contexts, in Refs. 9 and 37. The comparison of results shown in Figs. 10 and 11 show that, in order to get almost the same damping factor, larger feedback gains in lagging than in flapping are needed.

Related to the implementation of the proportional feedback control strategy, results not displayed here reveal that this strategy does not provide any substantial advantage as compared to that supplied by velocity feedback control. In addition, with that control methodology, there is no possibility to induce damping.

The effects of the feedback gain $\bar{K}_p$ and of the ply angle on the first two coupled frequencies of a pretwisted rotating blade ($\beta = 90$ deg and $\Omega = 100$ rad/s), are shown in Figs. 12 and 13. The results reveal the relatively modest effect played by the piezoelectric actuation.

In Figs. 14 and 15, the variation of the first two coupled flapping–lagging natural frequencies of the adaptive rotating blade as a function of the ply angle for prescribed values of the pretwist angle is supplied. The significant effect of ply angle on increasing the frequencies is worth noting. Moreover, the variation with β of natural frequencies is consistent, as it should be, with the trend emerging from Fig. 2.

In connection with one of the assumptions used in this paper, namely, that of invariability of the cross-sectional shape, although it is consistent with the requirement of preserving the original

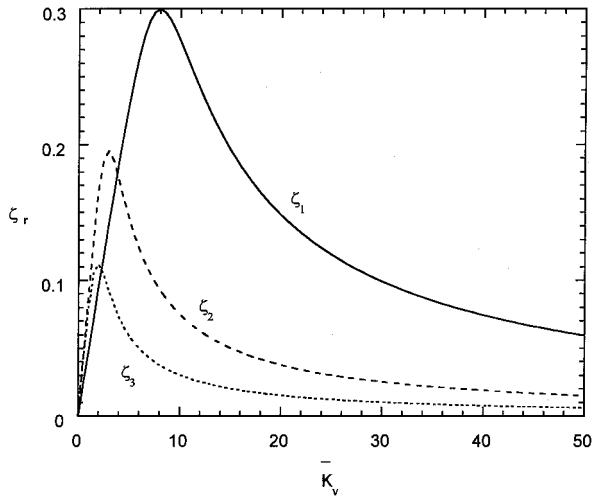

Fig. 10 Induced damping factors in flapping vs $\bar{K}_v$; $\theta = 0$ deg, $\beta = 0$ deg, and $\Omega = 0$.

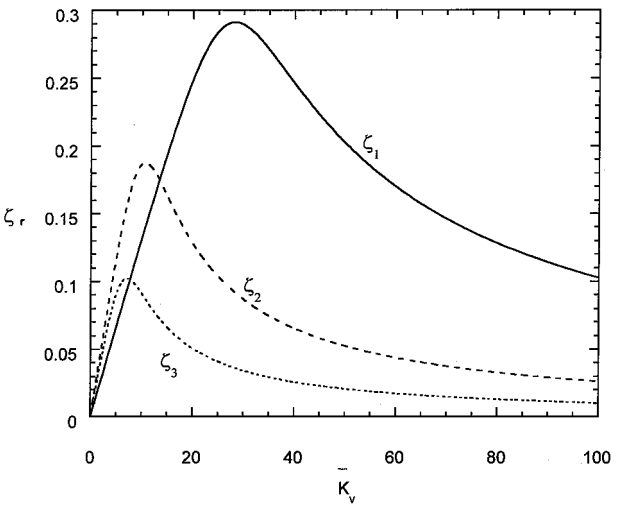

Fig. 11 Courterpart of Fig. 10 for the damping factor in lagging.

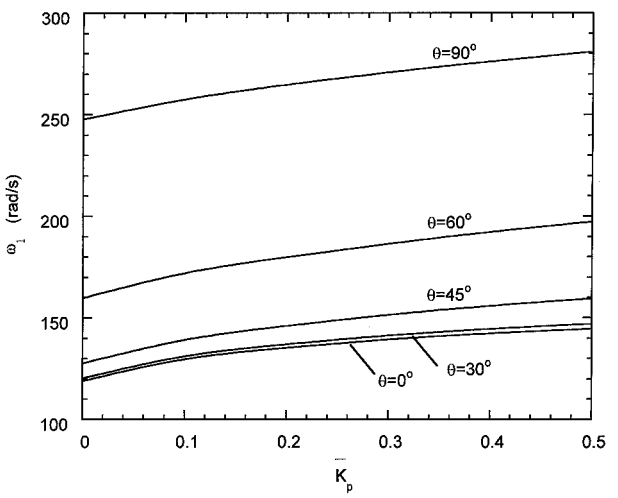

Fig. 12 Variation of the first coupled flapping–lagging natural frequency vs $\bar{K}_p$ for selected values of the ply angle; $\beta = 90$ deg and $\Omega = 100$ rad/s.

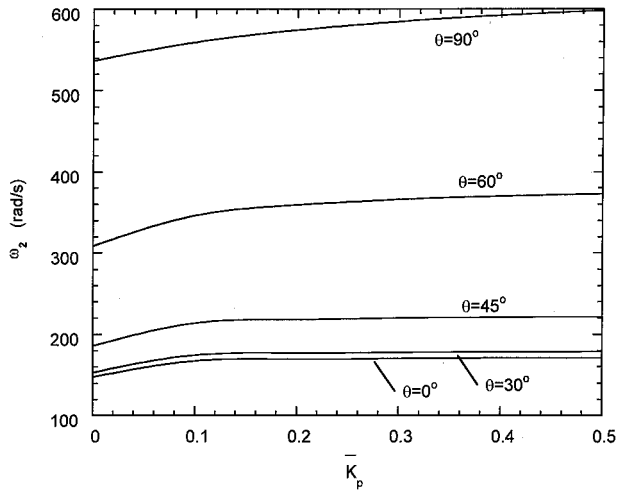

Fig. 13 Variation of the second coupled flapping–lagging natural frequency vs $\bar{K}_p$ for different ply angles; $\beta = 90$ deg and $\Omega = 100$ rad/s.

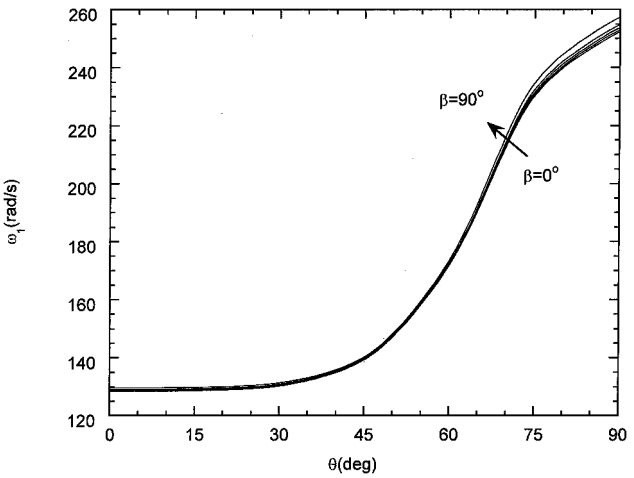

Fig. 14 Variation of the first coupled flapping–lagging natural frequency vs ply angle for selected values of the total pretwist angle; $\bar{K}_p = 0.1$ and $\Omega = 100$ rad/s.

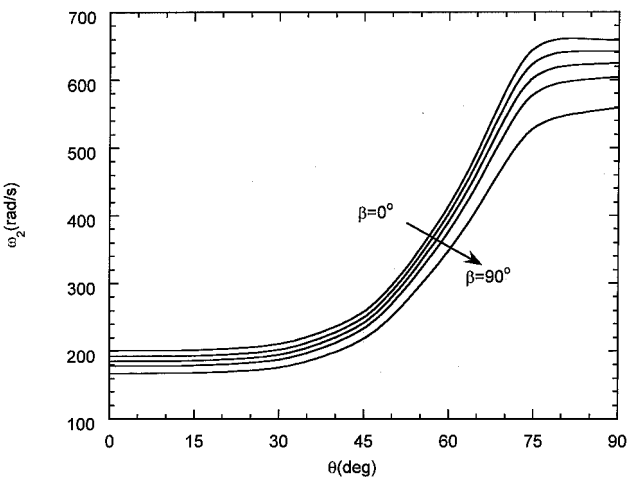

Fig. 15 Counterpart of Fig. 14 for the second coupled natural frequency.

aerodynamic features of the profile, in Ref. 38 it was shown, in an asymptotic sense, that for the CUS configuration beams this constraint does not result in overpredictions of related stiffness quantities.

Finally, note that in Ref. 39 the rotating box beam was modeled to include the bending–torsion elastic coupling via the implementation of the circumferentially asymmetric stiffness configuration.

Conclusions

A dynamic theory of rotating composite blades modeled as TWB of arbitrary cross section obtained via Hamilton's variational principle was supplied. The theory incorporates a number of nonclassical features that are essential for a reliable prediction of free-vibration characteristics of rotating composite blades. Among others, the theory includes transverse shear, anisotropy of constituent materials of the host structure, pretwist, and the adaptive control capability. The strong and synergistic effect played by the directionality property of advanced composite materials, considered in conjunction with that of piezoelectic actuation, on their dynamic response characteristics was highlighted. A powerful and robust solution methodology was used to determine both the open- and closed-loop free-vibration response characteristics. Although of a general character, in the sense of incorporating a number of essential non-classical features, the rotating blade model used can be extended further to include additional effects, for example, the presetting, precone, and cross-section nonuniformity. The results of such a generalization will be reported elsewhere.

Appendix: Expression of Global Stiffness Quantities Including the Pretwist Effect

The global stiffness quantities including the pretwist effect are

$$a_{22} = \left[m^2 a_{22}^p + n^2 a_{33}^p - 2mn a_{23}^p\right], \qquad a_{23} = mn\left[a_{22}^p - a_{33}^p\right]$$

$$a_{25} = a_{52} = \left[m^2 a_{25}^p - n^2 a_{34}^p + mn\left(a_{24}^p - a_{35}^p\right)\right]$$

$$a_{33} = \left[m^2 a_{33}^p + n^2 a_{22}^p + 2mn a_{23}^p\right]$$

$$a_{34} = a_{43} = \left[m^2 a_{34}^p - n^2 a_{25}^p + mn\left(a_{24}^p - a_{35}^p\right)\right]$$

$$a_{44} = \left[m^2 a_{44}^p + n^2 a_{55}^p - 2mn a_{45}^p\right]$$

$$a_{45} = mn\left[a_{44}^p - a_{55}^p\right], \qquad a_{55} = \left[m^2 a_{55}^p + n^2 a_{44}^p + 2mn a_{54}^p\right]$$

In addition, the mass terms are given by

$$b_1 = b_1^p, \qquad b_4 = m^2 b_4^p + n^2 b_5^p + 2mn b_6^p$$

$$b_5 = m^2 b_5^p + n^2 b_4^p - 2mn b_6^p, \qquad b_6 = mn\left[b_5^p - b_4^p\right]$$

$$b_{13} = mn\left[b_{14}^p - b_{15}^p\right], \qquad b_{14} = m^2 b_{14}^p + n^2 b_{15}^p - 2mn b_{13}^p$$

$$b_{15} = m^2 b_{15}^p + n^2 b_{14}^p + 2mn b_{13}^p$$

In these expressions, superscript p indicates that the symbols affected by it are associated with the beam cross section referred to the principal axes, x^p and y^p, whereas $m(Z) \equiv \cos\beta$ and $n(Z) \equiv \sin\beta$. The expressions of stiffness and mass terms referred to principal axes may be found in Ref. 6.

References

[1]Hodges, D. H., "Review of Composite Rotor Blade Modeling," *AIAA Journal*, Vol. 28, No. 3, 1990, pp. 561–565.

[2]Rosen, A., "Structural and Dynamic Behavior of Pretwisted Rods and Beam," *Applied Mechanics Reviews*, Vol. 44, No. 12, 1991, pp. 483–515.

[3]Ewins, D. J., and Henry, R., "Structural Dynamic Characteristics of Individual Blades," *Vibration and Rotor Dynamics*, Von Kármán Inst. for Fluid Dynamics, Lecture Series 1992-06, 1992, pp. 14.1–14.27.

[4]Kunz, D. L., "Survey and Comparison of Engineering Beam Theories for Helicopter Rotor Blades," *Journal of Aircraft*, Vol. 31, No. 3, 1994, pp. 473–479.

[5]Rand, O., "Analysis of Composite Rotor Blades," *Numerical Analysis and Modelling of Composite Materials*, edited by J. W. Bull, Blackie Academic and Professional, Chapman and Hall, London, 1996, pp. 1–26.

[6]Song O., and Librescu, L., "Free Vibration of Anisotropic Composite Thin-Walled Beams of Closed Cross-Section Contour," *Journal of Sound and Vibration*, Vol. 167, No. 1, 1993, pp. 129–147.

[7]Song, O., and Librescu, L., "Modeling and Vibration of Pretwisted Spinning Composite Thin-Walled Beams," *Proceedings of the 38th AIAA/ASME/ASCE/AHS/ASC Structures, Structural Dynamics, Materials Conference and Exhibition and AIAA/ASME/AHS/Adaptive Structures Forum*, Pt. 1, AIAA, Reston, VA, 1997, pp. 312–322.

[8]Song, O., and Librescu, L., "Structural Modeling and Free Vibration Analysis of Rotating Composite Thin-Walled Beams," *Journal of the American Helicopter Society*, Vol. 42, No. 4, 1997, pp. 358–369.

[9]Song, O., and Librescu, L., "Modeling and Dynamic Behavior of Rotating Blades Carrying a Tip Mass and Incorporating Adaptive Capabilities," *Acta Mechanica*, Vol. 134, 1999, pp. 169–197.

[10]Librescu, L., Meirovitch, L., and Song, O., "Integrated Structural Tailoring and Control Using Adaptive Materials for Advanced Aircraft Wings," *Journal of Aircraft*, Vol. 33, No. 1, 1996, pp. 203–213.

[11]Song, O., and Librescu, L., "Anisotropy and Structural Coupling on Vibration and Instability of Spinning Thin-Walled Beams," *Journal of Sound and Vibration*, Vol. 204, No. 3, 1997, pp. 477–494.

[12]Librescu, L., Meirovitch, L., and Na, S. S., "Control of Cantilever Vibration via Structural Tailoring and Adaptive Materials," *AIAA Journal*, Vol. 35, No. 8, 1997, pp. 1309–1315.

[13]Librescu, L., "Elasto-Statics and Kinetics of Anisotropic and Heterogeneous Shell-Type Structures," Noordhoff International, Leyden, The Netherlands, 1975, Chap. 3.

[14]Kosmatka, J. B., "Extension–Bend–Twist Coupling Behavior of Nonhomogeneous Anisotropic Beams with Initial Twist," *AIAA Journal*, Vol. 30, No. 2, 1992, pp. 519–527.

[15]Atilgan, A. R., and Rehfield, L. W., "Vibrations of Composite Thin-Walled Beams with Designed-in Elastic Couplings," *Achievements in Composites in Japan and United States*, edited by A. Kobayashi, *Proceedings of the Fifth Japan–U.S. Conference on Composite Materials*, Kokon Shoin Co., Ltd., Tokyo, 1990, pp. 687–694.

[16]Smith, E. C., and Chopra, I., "Formulation and Evaluation of an Analytical Model for Composite Box-Beams," *Journal of the American Helicopter Society*, Vol. 36, No. 3, 1991, pp. 36–47.

[17]Hodges, D. J., Atilgan, A. R., Cesnik, C. E. S., and Fulton, M. V., "On a Simplified Strain Energy Function for Geometrically Nonlinear Behavior of Anisotropic Beams," *Composites Engineering*, Vol. 2, No. 5–7, 1992, pp. 513–526.

[18]Liao, C. L., and Dang, Y. H., "Structural Characteristies of Spinning Pretwisted Orthotropic Beams," *Computers and Structures*, Vol. 45, No. 4, 1992, pp. 715–731.

[19]Birman, V., "Analytical Models of Sandwich Plates with Piezoelectric Strip Stiffeners," *International Journal of Mechanical Sciences*, Vol. 36, No. 6, 1994, pp. 567–578.

[20]Lin, C. Y., and Crawley, E. F., "Aeroelastic Actuation Using Elatic and Induced Strain Anisotropy," *Journal of Aircraft*, Vol. 32, No. 5, 1995, pp. 1130–1137.

[21]Librescu, L., and Na, S. S., "Boundary Control of Free and Forced Oscillation of Shearable Thin-Walled Beam Cantilevers," *European Journal of Mechanics A/Solids,* Vol. 17, No. 4, 1998, pp. 687–700.

[22]Librescu, L., Song, O., and Kwon, H. D., "Vibration and Stability Control of Gyroelastic Thin-Walled Beams via Smart Materials Technology," *Smart Structures*, edited by J. Holnicki-Szulk and J. Rodellar, NATO Science Series, 3 High Technology, Vol. 65, Kluwer Academic, Dordrecht, The Netherlands, 1999, pp. 163–172.

[23]Lagnese, J. E., and Lions, J. L., "Boundary Stabilization of Thin Plates," *SIAM Studies in Applied Mechanics*, Society for Industrial and Applied Mathematics, Philadelphia, 1989, Chap. 1.

[24]Baz, A., "Dynamic Boundary Control Beams Using Active Constrained Layer Damping," *Journal of Vibration and Acoustics*, Vol. 119, April 1997, pp. 166–172.

[25]Dosch, J. J., Inman, D. J., and Garcia, E., "A Self-Sensing Piezoelectric Actuator for Collocated Control," *Journal of Intelligent Material Systems Structures*, Vol. 3, 1992, pp. 166–184.

[26]Berlincourt, D. A., Curran, D. R., and Jaffe, H., "Piezoelectric and Piezomagnetic Materials and Their Function in Transducers," *Physical Acoustics—Principles and Methods,* edited by E. F. Mason, Vol. 1, Pt. A, Academic, New York, 1964, pp. 202–204.

[27]Subrahmanyam, K. B., and Kaza, K. R. V., "Vibration and Buckling of Rotating Pretwisted, Preconed Beams Including Coriolis Effects," *Journal of Vibration, Acoustics, Stress and Reliability in Design,* Vol. 108, April 1986, pp. 140–149.

[28]Surace, G., Anghel V., and Mares, C., "Coupled Bending-Bending-Torsion Vibration Analysis of Rotating Pretwisting Blades: An Integral Formulation and Numerical Examples," *Structural Dynamics—EURODYN '96*, edited by B. Augusti, M. Borri, and R. Spinelli, Balkema, Rotterdam, The Netherlands, 1996, pp. 1149–1153.

[29]Subrahmanyam, K. B., Kulkarni, S. V., and Rao, J. S., "Coupled Bending–Bending Vibrations of Pretwisted Blading Allowing for Shear Deformation and Rotary Inertia by the Reissner Method," *International Journal of Mechanical Sciences,* Vol. 23, No. 9, 1981, pp. 517–530.

[30]Slyper, H. A., "Coupled Bending Vibrations of Pretwisted Cantilever Beams," *Journal of Mechanical Engineering Science*, Vol. 4, No. 4, 1962, pp. 365–379.

[31]Carnegie, W., and Thomas, J., "The Effects of Shear Deformation and Rotary Inertia on the Lateral Frequencies of Cantilever Beams in Bending," *Journal of Engineering for Industry*, Vol. 94, Feb. 1972, pp. 267–278.

[32]Sabuncu, M., "Coupled Vibration Analysis of Blades with Angular Pretwist of Cubic Distribution," *AIAA Journal*, Vol. 23, No. 9, 1985, pp. 1424–1430.

[33]Lin, S. M., "Vibration of Elastically Restrained Nonuniform Beams with Arbitrary Pretwist," *AIAA Journal*, Vol, 35, No. 11, 1997, pp. 1681–1687.

[34]Balhaddad, A. S., and Onipede, D. Jr., "Three-Dimensional Free Vibration of Pretwisted Beams," *AIAA Journal*, Vol. 36, No. 8, 1998, pp. 1524–1528.

[35]Boyce, W. E., "Effect of Hub Radius on the Vibration of a Uniform Bar," *Journal of Applied Mechanics,* Vol. 23, No. 2, 1956, pp. 287–290.

[36]Librescu, L., Meirovitch, L., and Song, O., "Refined Structural Modeling for Enhancing Vibrational and Aeroelastic Characteristics of Composite Aircraft Wings," *La Recherche Aerospatiale,* Vol. 2, No. 1, 1996, pp. 23–35.

[37]Tzou, H. S., *Piezoelectric Shells: Distributed Sensing and Control of Continua*, Kluwer, Dordrecht, The Netherlands, 1993.

[38]Volovoi, V. V., Hodges, D. H., Cesnik, C. E. S., and Popescu, B., "Assessment of Beam Modeling Methods for Rotor Blade Application," *Proceedings of the 55th Annual Forum of the American Helicopter Society*, American Helicopter Society, Alexandria, VA, 1999.

[39]Chandra R., and Chopra, I., "Experimental-Theoretical Investigation of the Vibration Characteristics of Rotating Composite Box Beams," *Journal of Aircraft*, Vol. 29, No. 4, 1992, pp. 657–664.

A. M. Baz
Associate Editor